IEEE Access
Multidisciplinary | Rapid Review | Open Access Journal

Received February 18, 2021, accepted March 11, 2021, date of publication March 15, 2021, date of current version March 23, 2021.

Digital Object Identifier 10.1109/ACCESS.2021.3066091

An Adaptive Bidirectional Multibeam High-Altitude Platforms Aeronautical Telecommunication Network Using Dual Concentric Conical Arrays

YASSER ALBAGORY
Department of Computer Engineering, College of Computers and Information Technology, Taif University, Taif 21944, Saudi Arabia
e-mail: y.albagory@tu.edu.sa

This work was supported by Taif University Researchers Supporting Project number (TURSP-2020/161), Taif University, Taif, Saudi Arabia.

ABSTRACT An efficient aeronautical telecommunication network (ATN) is proposed in this article based on adaptive multibeam antenna arrays and high-altitude platforms (HAPs). First, the network structure is demonstrated, and its geometry is analyzed based on a geocentric coordinate system that converts the global positioning system (GPS) and altitude data of aircrafts and HAPs into direction-of-arrival (DOA) information which is required for subsequent beamforming operation. The antenna array is then formed by designing a low-profile dual concentric conical array (DCCA) with uniform elements distribution and is used at the aircraft and HAP to achieve bidirectional beamforming. The antenna array elements are fed by an adaptive-exponent sine profile function to reduce the sidelobe levels while the low-profile dual conical array structure reduces the secondary major lobe and backlobe levels. The proposed beamforming technique is also capable of providing multibeam towards several aircrafts at the same time for effective resource sharing and management. The radiation performance of the array is demonstrated, analyzed, and compared with the concentric circular array where it is found that the secondary major lobe has been reduced by 13 dB with sidelobe level down to −40 dB relative to the mainlobe level. In addition, the bit energy-to-noise power spectral density and probability of bit error of the proposed aeronautical network has been investigated at different operating frequencies including 3.5 GHz and millimeter wave (mm-wave) frequencies of 28 and 39 GHz. The simulation results have shown that a channel capacity of about 3 Gbps can be achieved for BPSK and QPSK signals using bidirectional beamforming for a channel bandwidth of 400 MHz at 28 and 39 GHz mm-wave frequencies while it is about 773 Mbps at 3.5 GHz for 100 MHz bandwidth that can be provided over a line-of-sight distance of 896 km between an aircraft and HAP.

INDEX TERMS Adaptive arrays, aeronautical telecommunication network, conical arrays, high-altitude platforms.

I. INTRODUCTION

A. BACKGROUND

Aeronautical telecommunication network (ATN) is one of the most growing and demanding communication systems in recent years due to the huge growth in aviation industry [1]–[9]. Although ATN was mainly directed to aircraft operational safety and control traffic, passengers onboard aircrafts can be provided by continuous Internet connectivity with high data rates to enjoy different services during flight. There is a continuous need to increase the connection speed and stability in ATN to achieve more efficient aircraft safety, help fast expectation of any sudden failure in aircraft subsystems, and keep the crew in contact with nearby airport or rescue facilities at any time. When a high data rate ATN connection is provided for aircrafts, this helps exchange extensive aircraft sensor data with more measurements, and hence, efficient real-time monitoring can be achieved. Even in situations like aircraft system complete failure, the exact location of aircraft can be determined, and as much possible rescue

The associate editor coordinating the review of this manuscript and approving it for publication was Hasan S. Mir.

can be provided. High data rate ATN also helps passengers to spend their inflight time in processing and following up their businesses or even for entertainment. However, the high speed of aircrafts and different regions they span make a challenge to design efficient globally cooperative ATNs to provide continuous inflight high-speed Internet connectivity.

Several communication systems have been designed and adapted for ATN such as air-to-ground (ATG) [10], air-to-air (A2A) [11]–[16] and satellite networks [17], [18]. In ATG networks, an aircraft can be connected to some commercial terrestrial cellular networks which direct signals to sky for aircrafts. The high speed of aircrafts and long-haul flights result in frequent handovers in ATG systems. In addition, the data rates provided through ATG systems are very limited. For example, the Gogo ATG-4 system [19] can provide maximum 9.8 Mbps for downloading, however practically, it falls to some fractions of 1 Mbps and can serve limited number of onboard passengers. Therefore, Gogo has moved to Ku-band satellites to provide higher download speeds of up to 60 Mbps while the uplink from aircrafts can be provided by the conventional ground ATG network. On the other hand, Nokia has provided broadband ATG connection with long-term evolution (LTE) mobile network that could provide link speeds up to 75 Mbps [20]. On the other hand, the A2A network is also proposed without ground or satellite support [11]–[16] where the network is based on ad-hoc aircraft-to-aircraft connection strategy over the L-band. However, the A2A network is very sensitive to aircrafts availability for providing continuous connection with the network. For global ATN coverage in regions where no ATG or A2A networks exist such as over oceanic or very wide deserts, mobile satellite systems provide the only existing coverage solution.

Satellite systems such as Inmarsat [21], OneWeb [22], and Starlink [23] are some examples of systems which can provide limited inflight Internet speeds. However, the high orbital speed of satellites forces the occurrence of frequent handovers especially for long-haul flights which increases the system complexity and operation.

Recently, the idea of using stratospheric high-altitude platform (HAP) [24] gains attention for aviation systems where the global wide coverage advantage of satellite systems at fixed station position could improve the system performance and help increase the data rates especially at millimeter wave (mm-wave) bands. HAPs fly at a quasi-stationary position of about 20 km high in the stratosphere and provides very wide coverage area approaching 1000 km diameter for ground receivers with very optimistic communication performance relative to both terrestrial cellular systems and satellites systems of any orbit altitude [24]–[28]. HAP can be utilized as a flying basestation to provide aircrafts with high-speed data connectivity and a network of HAPs can provide continuous coverage over oceanic and wide desert regions like satellite systems.

Therefore, HAP is expected to close the gap between different conventional ground and satellite ATNs and become the candidate of future high-speed Internet aeronautical network. On the other hand, at mm-wave bands, the communication link between aircrafts and HAP suffers from high atmospheric losses [24] and needs efficient radio resource management especially for the long-range connection between aircrafts and HAPs.

B. CONTRIBUTIONS

The ambitious features of HAPs for aeronautical networks are very encouraging, and therefore, this article has worked on improving the communication link performance in the network to efficiently provide high-speed data connectivity. The propagation channel between an aircraft and HAP is improved by proposing an adaptive beamforming technique which provides narrow beams for the communication link between aircrafts and HAPs and is performed at each of them in a bidirectional fashion to boost the desired signals and reduce the interference to other frequency sharing systems.

The HAP ATN is first investigated and geometrically analyzed to make use of the continuously measured data at aircrafts such as the global positioning system (GPS) location and altitude which will be mapped to the essential direction-of-arrival (DOA) information required in beamforming operation based on geocentric coordinate system without performing extensive-processing DOA algorithms. The antenna array is then designed to provide low sidelobes and backlobes levels with low secondary major lobe level by using uniform low-profile dual concentric conical array (DCCA) with adaptive-exponent sine tapered feeding profile function.

The HAP ATN radio resource management is further improved by generating multibeam radiation pattern at HAP which effectively share the same radio channel between several aircrafts. This multibeam can be also generated at aircraft during the handover process to provide seamless transition of service between HAPs and aircraft. Finally, the impact of pointing errors in mainlobe orientation at either an aircraft or HAP is investigated where the proposed beamforming has an important role in mitigating this problem by adapting the mainlobe direction to maintain continuous communication link with the minimum probability of bit error.

C. PAPER ORGANIZATION

After Section I, the HAP ATN system architecture is investigated in Section II while Section III establishes the HAP localization service table for aircrafts. In Section IV, the DCCA and beamforming technique are proposed and demonstrated, and Section V discusses the communication link performance of the HAP ATN. Finally, Section VI concludes the paper.

II. HAP ATN ARCHITECTURE

The communication environment between an aircraft and HAP is very attractive to build an efficient and high-speed network with minimal atmospheric and propagation losses especially for frequencies below 10 GHz [24]. This network can be further improved by adopting narrow-beam cellular

communications between aircrafts and HAPs. The network basestations are formed by HAPs while the aircrafts are like mobile users. Above clouds, and during stable cruise-height flights, the aircraft acts as a local basestation for onboard passengers. They can enjoy high-speed Internet if the communication link between the aircraft and HAP is maintained at the proper level of performance, and to achieve this objective, there should be a powerful connection provided by high-gain beams from the aircraft to HAP and vice versa. These high-gain beams should be provided at both ends to achieve maximum performance, and at the same time, high spectral efficiency through frequency reuse where the same spectrum can be reused at different directions with sufficient angular separation.

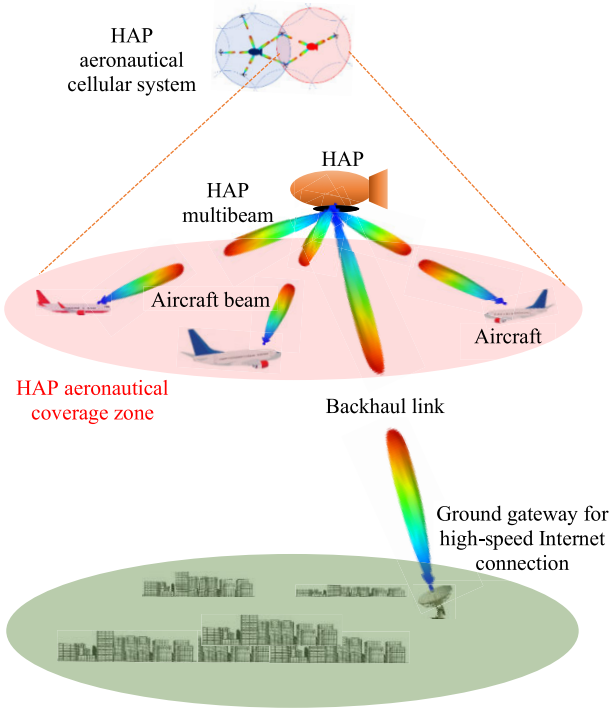

FIGURE 1. Bidirectional multibeam aeronautical HAP network.

Also, a HAP can direct multiple beams of the same radio resource to different aircrafts according to the location of each of them. In the overlapping regions between HAPs, an aircraft can communicate to the network through multiple beams to different HAPs according to the co-channel interference level and seamlessly perform handovers. The system can therefore be represented as shown in Fig. 1 which explore the dual-multibeam communication scenario between aircrafts and HAPs. The system management is expected to be much easier than performed in terrestrial mobile communications systems because airflights can be easily scheduled, managed, and the location of each aircraft is a deterministic variable. Also, the locations of HAPs are almost fixed in the network which simplifies the processing requirements for aircraft to track HAPs. Information like flight schedules and GPS location and altitude is essential in managing the proposed bidirectional-multibeam strategy.

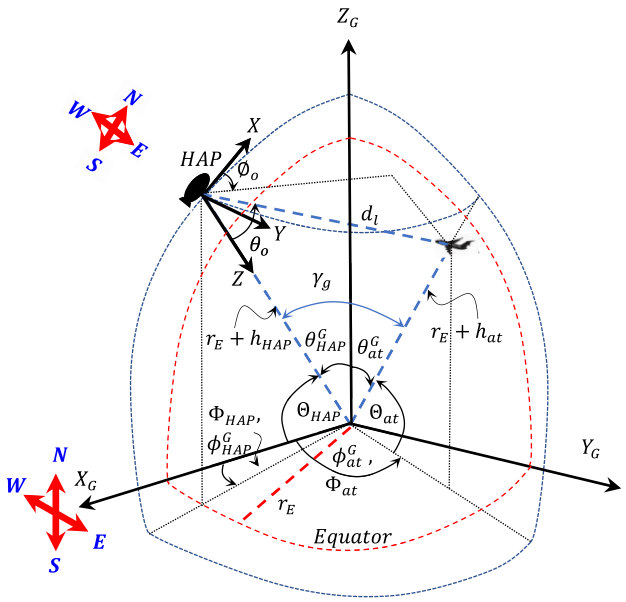

FIGURE 2. Geocentric coordinate system for aircraft-HAP aeronautical network.

III. ESTABLISHING HAP LOCALIZATION SERVICE TABLE FOR AIRCRAFTS

A. GEOCENTRIC COORDINATE SYSTEM FOR HAP ATN

The minimum required information by the aircraft and HAP are their global positioning system (GPS) locations and altitudes to establish proper connection and networking between them. Based on the GPS information, each HAP can serve any directly seen aircraft located inside its service area which can be determined according to maximum "line-of-sight" (LOS) distance to an aircraft at a certain altitude. The communication link distance between an aircraft and HAP can be determined from their GPS location information. The geometry in Fig. 2 maps the GPS latitude and longitude information (Θ, Φ) into geocentric spherical coordinates (θ^G, ϕ^G) as follows:

$$\theta^G = \begin{cases} 90 - \Theta & \text{in the northern hemesphere} \\ 90 + \Theta & \text{in the southern hemesphere} \end{cases} \quad (1)$$

and

$$\phi^G = \begin{cases} \Phi & \text{in the eastern hemesphere} \\ 360 - \Phi & \text{in the western hemesphere} \end{cases} \quad (2)$$

Therefore, the two GPS locations are mapped into two points of different radial distances according to their altitudes.

Assuming that the geographical latitude and longitude of the aircraft and HAP are (Θ_{at}, Φ_{at}) and $(\Theta_{HAP}, \Phi_{HAP})$ respectively, then the link distance can be calculated by:

$$d_l = \sqrt{(x_{HAP} - x_{at})^2 + (y_{HAP} - y_{at})^2 + (z_{HAP} - z_{at})^2} \quad (3)$$

and

$$x_{HAP} = (r_E + h_{HAP}) \cos(\phi^G_{HAP}) \sin\left(\theta^G_{HAP}\right) \quad (4)$$

$$y_{HAP} = (r_E + h_{HAP}) \sin(\phi^G_{HAP}) \sin\left(\theta^G_{HAP}\right) \quad (5)$$

$$z_{HAP} = (r_E + h_{HAP}) \cos\left(\theta^G_{HAP}\right) \quad (6)$$

$$x_{at} = (r_E + h_{at}) \cos(\phi^G_{at}) \sin\left(\theta^G_{at}\right) \quad (7)$$

$$y_{at} = (r_E + h_{at}) \sin(\phi^G_{at}) \sin\left(\theta^G_{at}\right) \quad (8)$$

$$z_{at} = (r_E + h_{at}) \cos\left(\theta^G_{at}\right) \quad (9)$$

where r_E is the earth radius, h_{at} and h_{HAP} are the aircraft and HAP altitudes respectively, (x_{at}, y_{at}, z_{at}) and $(x_{HAP}, y_{HAP}, z_{HAP})$ are the aircraft and HAP geocentric Cartesian coordinates, respectively.

The link distance has an upper limit at which it almost tangent to the Earth's surface and is given by:

$$d_{lMAX} = \sqrt{h_{HAP}(h_{HAP} + 2r_E)} + \sqrt{h_{at}(h_{at} + 2r_E)} \quad (10)$$

d_{lMAX} refers to the longest LOS distance between an aircraft and HAP before complete blocking from the earth surface occurs. It also defines the range of visible GPS locations of aircrafts to HAP. The corresponding maximum ground angle γ_{gMAX} is given by:

$$\gamma_{gMAX} = \tan^{-1}\left(\frac{\sqrt{h_{HAP}(h_{HAP} + 2r_E)}}{h_{HAP} + r_E}\right) + \tan^{-1}\left(\frac{\sqrt{h_{at}(h_{at} + 2r_E)}}{h_{at} + r_E}\right) \quad (11)$$

Therefore, the available aircraft service localization table can be determined from the GPS location of a HAP as follows:

$$\Theta_{at} = \Theta_{HAP} \pm \gamma_{gMAX} \left|\sin(|\Delta\Phi| - \gamma_{gMAX})\right|, \quad (12)$$

where $0 \le |\Delta\Phi| \le \gamma_{gMAX}$ and

$$\Phi_{at} = \Phi_{HAP} \pm \gamma_{gMAX} \left|\sin(|\Delta\Theta| - \gamma_{gMAX})\right|, \quad (13)$$

where $0 \le |\Delta\Theta| \le \gamma_{gMAX}$ and $|\Delta\Theta| = |\Theta_{HAP} - \Theta_{at}|$ and $|\Delta\Phi| = |\Phi_{HAP} - \Phi_{at}|$ taking into consideration the geographical directions.

The formula (12) and (13) can be applied if the difference in latitudes and/or longitudes is less than γ_{gMAX} which means that the aircraft lies in the HAP service area. The service availability from a HAP depends on the inequalities of (12) and (13) where at least one of them should be satisfied. For example, if the maximum aircraft height is 11 km while the HAP is positioned at 20 km high, then $d_{lMAX} \approx 880$ km from (10) and the corresponding latitude and longitude limits are:

$$\Theta_{at} = \Theta_{HAP} \pm 8.0479^\circ \left|\sin\left(|\Delta\Phi| - 8.0479^\circ\right)\right|, \quad 0 \le |\Delta\Phi| \le 8.0479^\circ \quad (14)$$

$$\Phi_{at} = \Phi_{HAP} \pm 8.0479^\circ \left|\sin\left(|\Delta\Theta| - 8.0479^\circ\right)\right|, \quad 0 \le |\Delta\Theta| \le 8.0479^\circ \quad (15)$$

Therefore, for any HAP, there is a set of visible aircraft GPS locations that can be served by this HAP which can be recorded in its service table for proper resource management. The service tables of neighbored HAPs in a cellular HAP ATN should have some shared aircraft GPS locations in the overlapped areas which is necessary during handover operation between aircrafts and HAPs. In addition, for an aircraft, the service localization coordinates from (12) and (13) should be updated continuously during flight and if any HAP has moved to another location, the whole network should be informed by the new HAP GPS and localization table.

B. MAPPING OF GPS DATA INTO DOA INFORMATION

The GPS data received from an aircraft is very useful for directing high-gain beams from HAP to this aircraft which reduces the processing load required to find the aircraft DOA. Accurate GPS information will lead to an optimum transmission of signals in the system where the maximum power radiated/received will be always directed toward the aircraft. As the GPS data is changing during flight, the mainlobe direction should be adapted also. Therefore, the GPS data can be mapped directly to DOA information which represent the mainlobe direction at the antenna array end.

Consider the geometry shown in Fig. 2, if the HAP X-axis is maintained pointing to the North direction, then the Y-axis represents the East, and the Z-axis is pointing to earth's center. The extension of aircraft location at the same HAP height (Point A), HAP (point H) and the point V form a spherical triangle in which the following relation holds:

$$\frac{\sin(\emptyset_o)}{\sin(\theta_{at})} = \frac{\sin(\emptyset_{at} - \emptyset_{HAP})}{\zeta} \quad (16)$$

$$\text{where } \zeta = \sqrt{\kappa_1^2 + \kappa_2^2 + \kappa_3^2} \quad (17)$$

and

$$\kappa_1 = \cos\left(\phi^G_{HAP}\right) \sin\left(\theta^G_{HAP}\right) - \cos(\phi^G_{at}) \sin\left(\theta^G_{at}\right) \quad (18)$$

$$\kappa_2 = \sin\left(\phi^G_{HAP}\right) \sin\left(\theta^G_{HAP}\right) - \sin(\phi^G_{at}) \sin\left(\theta^G_{at}\right) \quad (19)$$

$$\kappa_3 = \cos\left(\theta^G_{HAP}\right) - \cos(\theta^G_{at}) \quad (20)$$

Therefore, the azimuth DOA of the aircraft at HAP is given by:

$$\phi_o = \sin^{-1}\left(\frac{\sin(\theta_{at})\sin(\emptyset_{at} - \emptyset_{HAP})}{\zeta}\right) \quad (21)$$

and the elevation DOA of the aircraft is given by:

$$\theta_o = \cos^{-1}\left(\frac{d_l^2 + h_{HAP}^2 - h_{at}^2 + 2r_E\,(h_{HAP} - h_{at})}{2d_l\,(r_E + h_{HAP})}\right) \quad (22)$$

The same procedure for obtaining $(\theta_o, \emptyset_o)$ of the aircraft at HAP can be followed to obtain the DOA information of the HAP at the aircraft to achieve bidirectional beamforming between them.

As a case study, consider an aircraft that has a location of $(30^\circ N, 30^\circ E)$ and flying at an altitude of 11 km is communicating with HAP that has a location of $(24^\circ N, 25^\circ E)$ with altitude of 20 km high, then according to (21) and (22), the DOA of the aircraft at HAP is $(85.6^\circ, 35.4^\circ)$. The DOA pair $(\theta_o, \emptyset_o)$ from (21) and (22) are now ready to be inserted in the

beamformer at HAP which will be described and discussed in the next section. One of the major considerations about mapping the GPS data to DOA information at the beamformer is the high sensitivity to the GPS measurements accuracy which will affect the accuracy of mainlobe orientation during connection. A 1° error in either latitude or longitude is equivalent to approximately 111 km error in location on the ground. So, the beamformer at either aircraft or HAP should rely on very accurate GPS measurements.

IV. ONBOARD BEAMFORMING USING LOW-PROFILE DUAL CONCENTRIC CONICAL ARRAY (DCCA)

A. SYSTEM REQUIREMENTS

In this section, we will utilize antenna arrays to generate adaptive high-gain narrow beams from aircrafts and HAPs. There are many antenna arrays structures that could be used, however, the proposed communication system in this article requires specific beam characteristics where the following requirements should be achieved:

1- Electronic steering of beams at any direction in a half-spherical solid angle.
2- Very low sidelobe levels.
3- Very low backward radiation.
4- Fast beam generation and adaptation with low processing requirements.
5- Mainlobe gain control.
6- Conformal array structure for aircrafts considering aerodynamics performance.

The above requirements are very necessary to achieve high performance communications which ensures high-speed Internet connectivity to aircrafts. The first two objectives can be achieved through simple phased two-dimensional arrays, while the second and third requirements need special antenna weighting where several optimization techniques can be applied [29]–[38]. The fourth requirement will focus on beamforming techniques that fast calculate and adapt the beam pattern through changing the weighting vector such as tapered beamforming. Therefore, optimization techniques that provide the lowest sidelobe levels through designing non-uniform arrays with extensive calculation and learning techniques to get the optimum weights will not be suitable in this case. The fifth requirement can be easily achieved by increasing or decreasing all weight values by the same factor to control the mainlobe gain toward the aircraft. And finally, the antenna arrays at the aircraft should be conformal to its surface and therefore low-profile structures should be used especially if it will be fixed on the aircraft fuselage.

B. DCCA STRUCTURE AND FEEDING PROFILE

As discussed in the previous section, to achieve the required mentioned objectives, we may design an antenna array structure at HAP which will be in the form of dual concentric conical arrays (DCCA) fixed at the bottom side of the platform in Fig. 1. In array signal processing, the adopted antenna elements in the array are assumed to be isotropic radiators which can be practically achieved by several crossed-dipole designs such as in [39]–[41] using half-wavelength dipoles or microstrip patch antennas. The crossed dipole (or turnstile antenna) has been specifically chosen to investigate the impact of the proposed array design and beamforming technique only without incorporating specific directional antenna radiation characteristics. This isotropic antenna can be supported by metallic ground plane at quarter wavelength separation distance to further reduce the backlobe radiation [42].

The array configuration has two low-profile concentric conical arrays of different base angles where the outer conical array has a higher base angle of 30° while it is 15° for the inner one. This array structure is proposed to reduce the backward radiation and provide very low sidelobe levels. The same structure can be used onboard an aircraft where it can be fixed on some partially spherical parts or can be fixed in a radome over the wings or even on the aircraft nose. The geometry of the HAP ATN indicates that it is always for HAP to form beams downward while for aircrafts it should form the beams in upward directions.

Array configurations such as spherical-cap array [38] can be also used, where it provides low backlobe radiation with low secondary lobes in their radiation pattern, however it suffers from wider beamwidths which reduces the efficiency of spatial connectivity between aircrafts and HAPs. The mostly related array configuration that can be compared with DCCA is the concentric circular array (CCA) [30]–[37], therefore, it will be compared in radiation performance with the proposed DCCA.

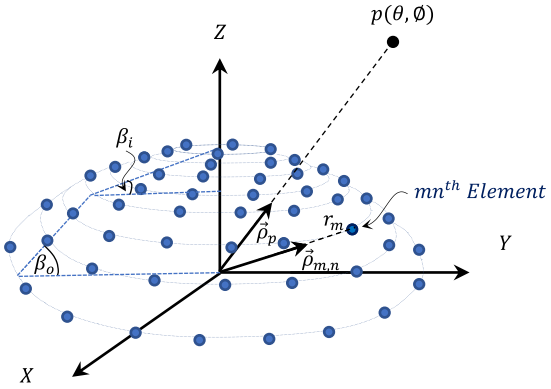

FIGURE 3. Geometrical structure projection in the *XZ*-plane of the dual concentric conical array (DCCA).

According to the geometry of the DCCA shown in Fig. 3, we can determine the array steering vector, which is formed by two sub-vectors, each corresponds to one of the conical arrays as follows:

$$\mathbf{\Gamma}(\theta, \phi) = \begin{bmatrix} \boldsymbol{\gamma}_o(\theta, \phi) \\ \boldsymbol{\gamma}_i(\theta, \phi) \end{bmatrix} \tag{23}$$

where $\boldsymbol{\gamma}_i(\theta, \phi)$ and $\boldsymbol{\gamma}_o(\theta, \phi)$ are the inner and outer conical arrays steering vectors formed by the sub circular arrays steering vectors, so, if the inner and outer conical arrays are formed by M_i and M_o coaxial circular arrays respectively, then each of them is formed by vertically concatenated sub-steering vectors where each corresponds to one of the circular

array in conical array. Therefore, the n^{th} element in the m^{th} vector will be given by:

$$c_{m,n}(\theta,\phi) = e^{\frac{j2\pi}{\lambda} r_m \vec{\rho}_p . \vec{\rho}_{m,n}} \tag{24}$$

where $m = 1, 2, \ldots, M$ is the index of the circular arrays with $M = M_i + M_o$ and $n = 1, 2, \ldots, N_m$ is the index of elements in the m^{th} circular array, $\vec{\rho}_p$ is a unit vector toward the observation point P and $\vec{\rho}_{m,n}$ is a unit vector toward the n^{th} element in the m^{th} circular array and r_m is the radial distance from the origin to the m^{th} circular array circumference.

The overall array factor can be written as follows:

$$G_c(\theta,\phi) = \mathbf{W}^H(\theta_o,\phi_o)\,\mathbf{\Gamma}(\theta,\phi) \tag{25}$$

where $\mathbf{W}^H(\theta_o,\phi_o)$ is the weight vector calculated for the mainlobe direction (θ_o,ϕ_o) where it is chosen to taper the currents of the m^{th} ring elements according to the following proposed profile:

$$\alpha_m = \left(\sin\left(\frac{\pi m}{2M}\right)\right)^{(\mu_T/100)} \tag{26}$$

where μ_T is the total number of elements in the array.

The array power gain is therefore given by:

$$A_p(\theta,\phi) = |G_c(\theta,\phi)|^2 \tag{27}$$

This proposed design of DCCA is expected to reduce the sidelobe levels and secondary major image lobe formed at $\theta > 90°$ for $\theta_o < 90°$. This secondary major lobe causes unwanted radiation toward sky when the beams are formed at HAP while for an aircraft, it is generated toward ground causing radio interference with terrestrial networks that may use the same frequency bands.

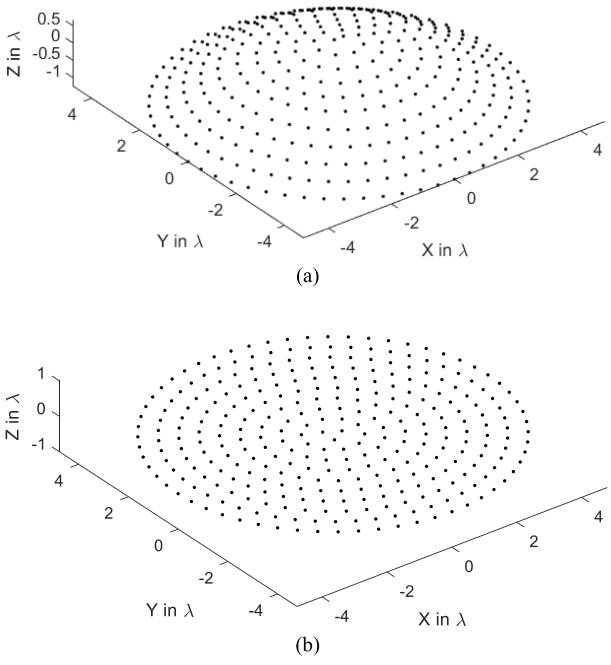

FIGURE 4. The array structures of (a) dual concentric conical array, (b) concentric circular array.

C. RADIATION PATTERN COMPARISON BETWEEN DCCA AND CONCENTRIC CIRCULAR ARRAY

To investigate the radiation patten characteristics of the DCCA, it will be compared with one of the most efficient planar arrays which is the concentric circular array. A DCCA is designed with two concentric conical arrays with base angles of 30° and 15° as shown in Fig. 4(a), with interior and exterior conical arrays are formed by uniformly spaced 5 rings for each. On the other hand, the concentric circular array is designed by setting the two base angles of the DCCA to 0° as shown in Fig. 4(b). The antenna elements in the two arrays are uniformly spaced by a half-wavelength distance. The proposed feeding profile in both arrays is given by:

$$w_m(\theta_o,\phi_o) = \left(\sin\left(\frac{\pi m}{2M}\right)\right)^{(\mu_T/100)} \Gamma_m(\theta_o,\phi_o) \tag{28}$$

where $\Gamma_m(\theta_o,\phi_o)$ is the m^{th} ring weighting vector and $\Gamma_m(\theta_o,\phi_o)$ is its corresponding steering vector determined at the mainlobe direction (θ_o,ϕ_o).

As shown in Fig. 5(a) and (b), the array 3D normalized power pattern is tested for a mainlobe formed at the direction $(40°, 150°)$ in the two array structures exploring one of the very important advantages of the proposed DCCA which is the reduction of the secondary major lobe. The planar structure of the concentric circular array results in a secondary major lobe of the same level as the mainlobe. Reducing image lobe is very important as it causes very high interference and degrades the system performance.

On the other hand, a more detailed normalized power pattern is shown in Fig. 6(a) and (b) for the two arrays and the normalized radiation pattern is viewed in the elevation and azimuth planes in Figs. 7(a), 7(b), 8(a), and 8(b) respectively to view the exact literal radiation levels.

In Figs. 7(a) and (b), the DCCA has a reduced secondary major lobe of -13 dB and a backlobe level of -25 dB relative to the mainlobe level, respectively. On the other hand, the concentric circular array in Figs. 8(a) and 8(b) provides 0 dB of secondary major lobe and a backlobe level of -25 dB.

The secondary major lobe in the concentric circular array is converted from a strong peak of equal level as the mainlobe to a lower level of radiation plateau in the DCCA at -13 dB level. Therefore, there is an advantage of 13 dB on using the DCCA compared to concentric circular array while the two structures almost provide the same backlobe level of -25dB. However, the concentric circular array provides a very deep sidelobe level of -50 dB while the dual concentric conical array has -40 dB, and although the concentric circular array provides very deep sidelobe levels, the proposed DCCA still provides a very acceptable sidelobe levels with the advantage of reduced secondary major lobe.

D. DCCA MULTIBEAM GENERATION AND PERFORMANCE

The multibeam connections with different aircrafts can be achieved by adjusting the weighting formula in (28) so that it becomes the sum of individual beam weights provided that the accumulated unwanted radiation levels do not affect

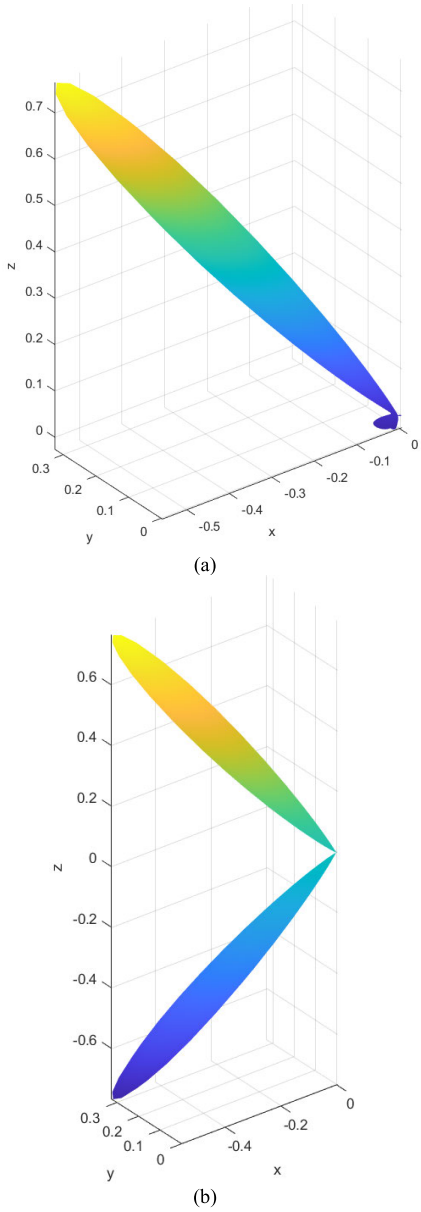

FIGURE 5. 3D normalized absolute power pattern of (a) dual concentric conical array, (b) concentric circular array.

the system performance. Therefore, the overall multibeam weight becomes:

$$\mathbf{W}_{I_b} = \sum_{i=1}^{I_b} \xi_i \mathbf{W}(\theta_i, \phi_i) \tag{29}$$

where I_b is the number of mainlobes required for establishing high-gain communication link with a number of I_b aircrafts and ξ_i is the i^{th} beam gain control factor. Fig. 9 displays the 3D power pattern of three mainlobes directed toward (85°, 150°), (85°, 210°), and (85°, 270°) with $\xi_i = 1$. The detailed normalized radiation levels are shown in Fig. 10 where the addition of the three individual weight vectors in (29) results in some increase in the backlobe levels which is raised to −10 dB. In these two figures, the elevation angle is chosen as the maximum allowable value where $\theta_{oMAX} = 85°$ which corresponds to a mainlobe directed to the farthest aircraft that

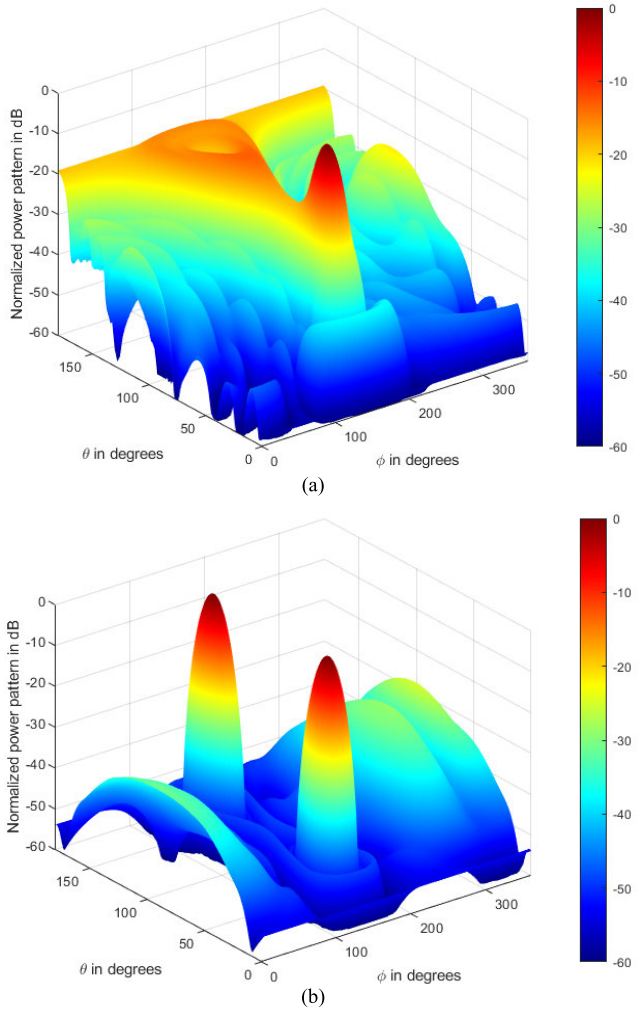

FIGURE 6. The normalized power pattern variation in dB with elevation and azimuth directions of (a) dual concentric conical array, (b) concentric circular array.

can be communicated with. The mainlobe at θ_{oMAX} has the widest beamwidth in the θ plane while the beams have almost constant beamwidths in the Ø plane.

On the other hand, the planar concentric circular array is compared for multibeam generation with the proposed dual concentric conical array for a sample of cogenerated three mainlobe levels at (40°, 30°), (40°, 150°), and (40°, 200°) with $\xi_i = 1$ and the 3D beam patterns are shown for the proposed DCCA and concentric circular array in Figs. 11(a) and 11(b) respectively which show the clearly reduced secondary major lobes in the DCCA pattern.

V. COMMUNICATION LINK PEROFMANCE OF HAP ATN

A. PERFORMANCE PARAMETERS AND AIRCRAFT-HAP FREQUENCY ZONE PLANNING

The beamforming technique described in the previous section provides narrow beams which can be generated at both aircraft and HAP, and in this case, the communication link can be seen as a dynamic LOS microwave link which effectively mitigates the fading effects, and the aircraft-HAP

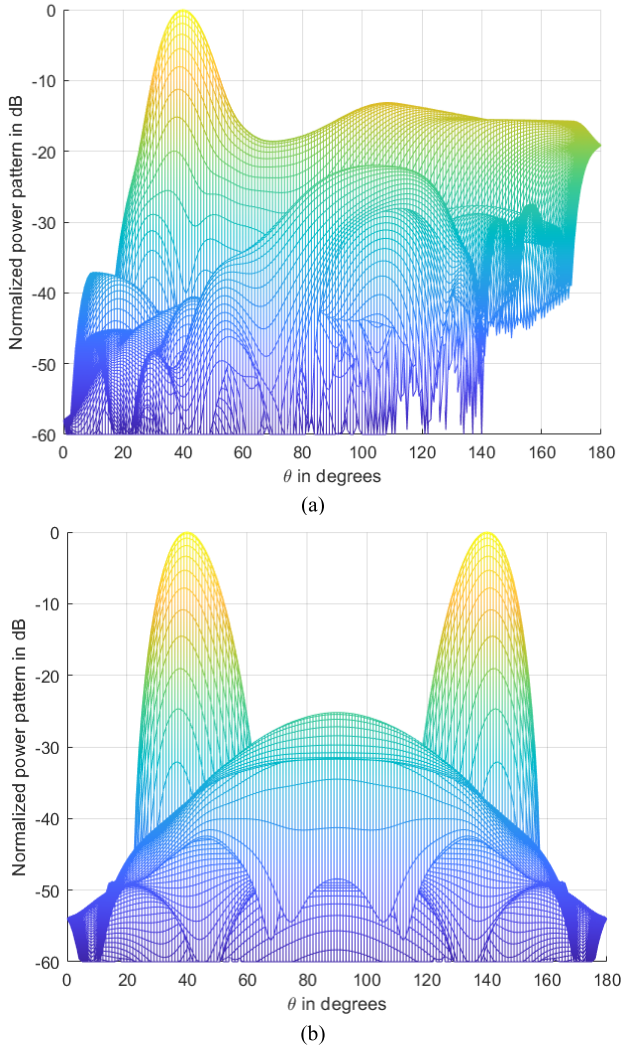

FIGURE 7. Projection of the normalized power pattern in dB with elevation angle (a) dual concentric conical array, (b) concentric circular array.

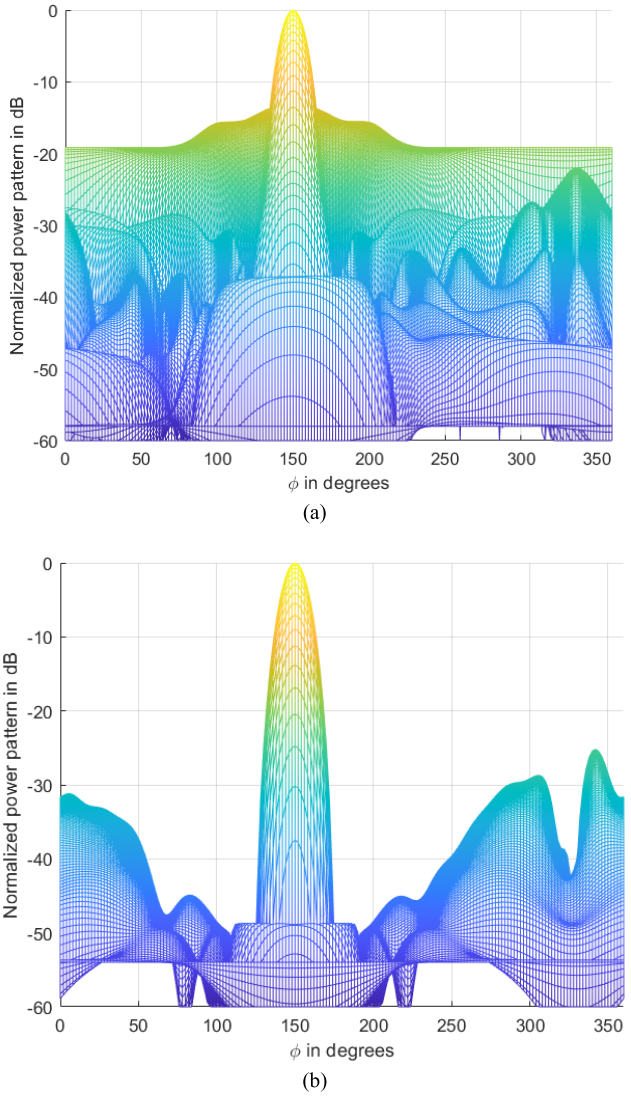

FIGURE 8. Projection of the normalized power pattern in dB with azimuth angle (a) dual concentric conical array, (b) concentric circular array.

system becomes single-input single-output if only one beam is generated from each station towards the other. Under these assumptions, we can determine the received signal power at the aircraft receiver, P_a, which is given by:

$$P_a(\theta,\phi) = A_{p|HAP}(\theta,\phi)\, A_{p|a}(\theta,\phi)\, P_{HAP}\left(\frac{\lambda}{4\pi d_l}\right)^2 \frac{1}{L_x} \quad (30)$$

where P_{HAP} is the HAP transmitted power, $A_{p|HAP}(\theta,\phi)$ and $A_{p|a}(\theta,\phi)$ are the antenna array power gains at the HAP and aircraft respectively, L_x is an extra loss due to atmospheric absorption losses, feeder losses, polarization loss, and any other losses, and $(\lambda/4\pi d_l)^2$ represents the free-space loss (FSL).

The bit energy-to-noise spectral density, $E_b(\theta,\emptyset)/N_o$, at the aircraft receiver is given by:

$$\frac{E_b(\theta,\emptyset)}{N_o} = \frac{P_a(\theta,\phi)}{N_o R_B} \quad (31)$$

where R_B is the bit rate and N_o is the noise power spectral density. For a communication channel of bandwidth B_w, the signal-to-noise ratio at the aircraft is:

$$\frac{S(\theta,\emptyset)}{N} = \frac{R_B E_b(\theta,\emptyset)}{B_w N_o} \quad (32)$$

or

$$\frac{S(\theta,\emptyset)}{N} = \frac{P_a(\theta,\phi)}{B_w N_o} \quad (33)$$

The probability of bit error is directly related to the value of $E_b(\theta,\emptyset)/N_o$ and the digital modulation scheme. For BPSK and QPSK, the spatial probability of bit error is given by [43]:

$$P_B(\theta,\emptyset) = \frac{1}{2} erfc\left(\sqrt{\frac{E_b(\theta,\emptyset)}{N_o}}\right) \quad (34)$$

where $erfc(x)$ is the complementary error function. According to the Shannon–Hartley theorem [39], the aircraft-HAP communication channel spatial capacity assuming additive white

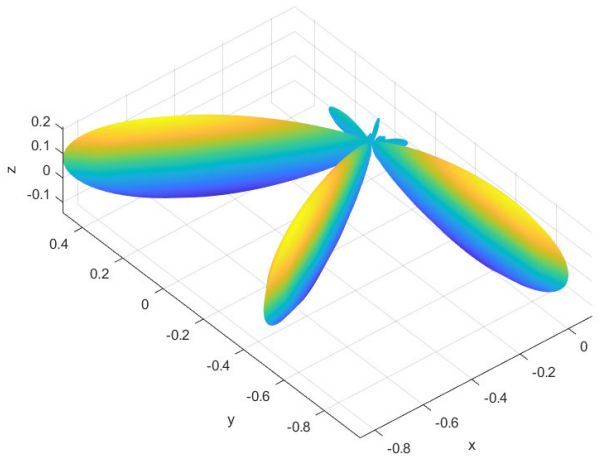

FIGURE 9. Three mainlobes generated from the multibeam dual concentric conical array directed toward the end-of-coverage aircrafts.

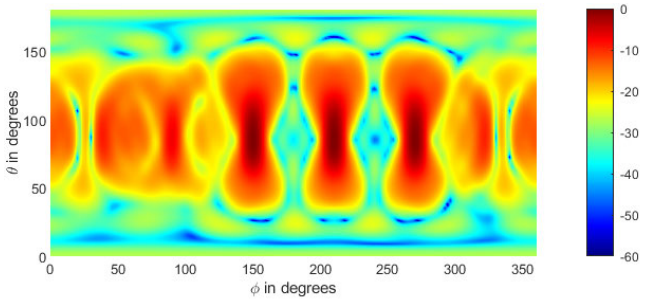

FIGURE 10. Normalized power pattern in dB of three mainlobes generated from the multibeam dual concentric conical array directed toward the end-of-coverage aircrafts.

gaussian noise (AWGN) channel which is bandlimited to B_w Hz- is given by:

$$C_{HAP}(\theta, \emptyset) = B_w \log_2 \left(1 + \frac{P_a(\theta, \phi)}{B_w N_o}\right) \text{bit/s} \qquad (35)$$

To demonstrate the communication link performance, the system spatial probability of error and capacity are displayed for the worst case of the link where the aircraft is located at the coverage boundary of the HAP area. The atmospheric loss variation with frequencies in [44], [45] has investigated that frequencies below 10 GHz suffers much less atmospheric losses than the higher mm-wave band frequencies, therefore, a carrier frequency of 3.5 GHz is suggested for providing reliable link performance for the aircrafts at the coverage boundary of the HAP where the atmospheric and FSL are highest and may become even worse during heavy rains. On the other hand, if the aircraft is flying above clouds and the complete LOS path to the HAP is passing above the troposphere, then we can utilize the higher mm-wave band frequencies such as 28 and 39 GHz where the atmospheric losses are very low, and it becomes feasible for aircraft communication. However, if the LOS passes again through the troposphere, the lower 3.5 GHz frequency should be used. Therefore, the HAP coverage area can be formed by two circular zones as shown in Fig. 12 with the suggested carrier

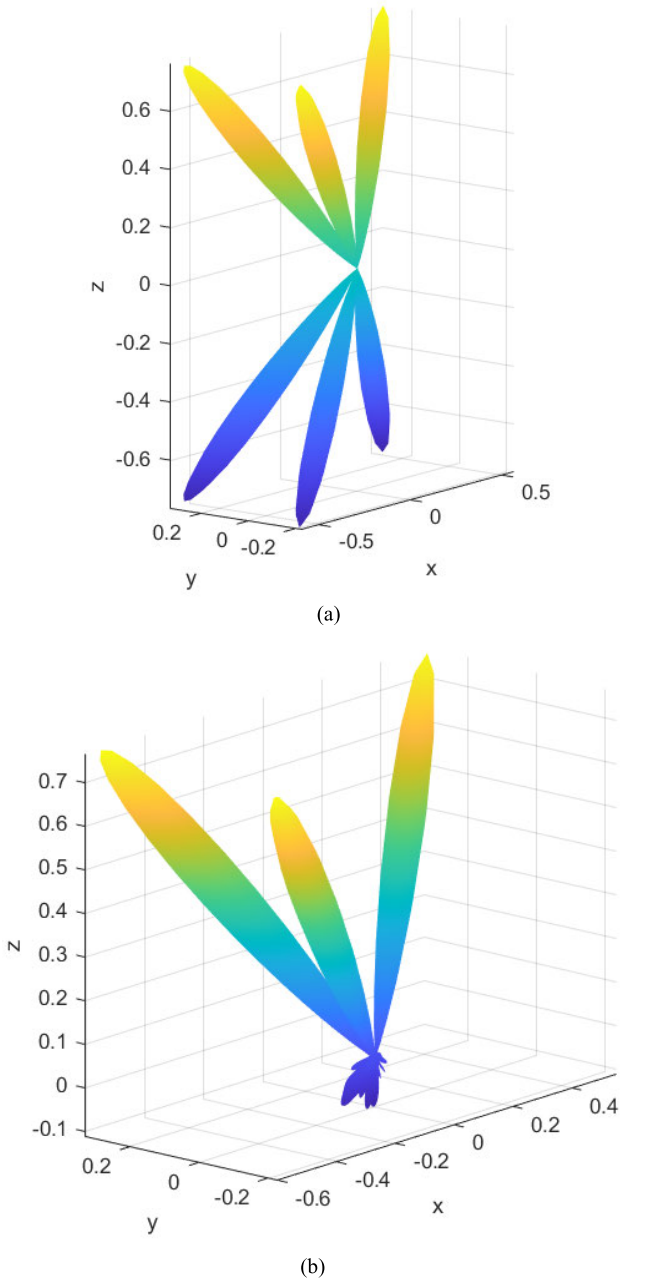

FIGURE 11. Three mainlobe cogenerated by (a) CCA, (b) DCCA.

distribution to provide the highest possible data rates at lowest atmospheric losses.

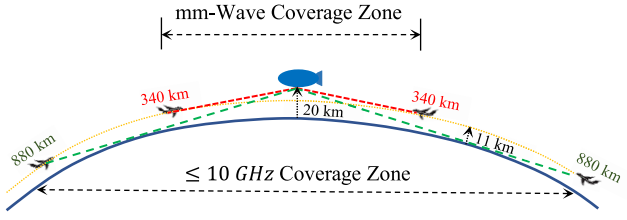

FIGURE 12. HAP aeronautical coverage zones base on frequency ranges.

Table 1 displays typical parameters and their values for examining the system performance using the proposed array

TABLE 1. HAP ATN operational parameters.

System parameter	Value
HAP altitude, h_{HAP}	20 km
Aircraft operational altitude, h_{at}	11 km
d_{lMAX}	880 km
d_{lMIN} (HAP at zenith direction of the aircraft)	9 km
Carrier frequencies	3.5, 28, and 39 GHz
Channel bandwidth, B_w	100 MHz @ 3.5 GHz 50 to 400 MHz @ 28 and 39 GHz
AWGN spectral density, $N_o = kT$	4.11×10^{-21} Watt/Hz
HAP transmitted power per channel, P_{HAP}	0.18 - 6 Watts (22.55 - 37.8 dBm)
Outer conical array base angle	30°
Inner conical array base angle	15°
M_o	5
M_i	6
Total number of elements in the array	348 elements
The outermost ring size,	60 elements
The innermost ring size	2 elements
Mainlobe direction, $(\theta_o, \emptyset_o)$	$(85°, 180°)$
Bit rate, R_B	Set to maximum theoretical limit (Shannon's capacity).
Aircraft antenna array configuration	Same as HAP (two-way beamforming)
Mainlobe gain in dB at HAP	38 dB
Mainlobe gain in dB at aircraft	38 dB
Link atmospheric losses in dB (clear sky)	2.8 dB @ 3.5 GHz 14 dB @ 28 GHz 26 dB @ 39 GHz
Free space loss in dB at the boundary of HAP coverage area	162.4 dB @ 3.5 GHz 180.4 dB @ 28 GHz 183.3 dB @ 39 GHz
Extra losses in dB	3 dB

and beamforming technique for the HAP-ATN. As listed in this table, the atmospheric losses for higher mm-wave frequencies are great and therefore, it is recommended only to use these frequencies for inflight cases where the LOS is totally above clouds as the atmospheric losses are only 0.25 and 0.55 dB for the 28 and 39 GHz frequencies respectively [24] for a link distance of 340 km.

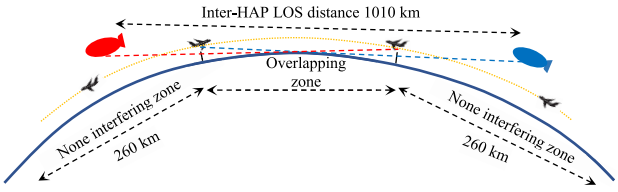

FIGURE 13. HAP ATN overlapping and none-interfering zones.

One of the interesting features when establishing cellular HAP ATN is the self-shadowing of earth to the propagated waves which efficiently prevent the co-channel interference between HAP aeronautical cells. The earth-self shadowing effect is shown in Fig. 13 where aircrafts can enjoy free-of-interference zone of about 260 km long centered under each HAP. The inter-HAP LOS link distance is about 1010 km which is required for continuous cellular coverage ATN based on HAPs only.

TABLE 2. Performance summary of HAP ATN.

Frequency, in GHz	3.5	28		39	
Channel bandwidth, B_w in MHz	100	50	400	50	400
Maximum communication range in km	896	340	340	340	340
Probability of bit error, P_B	$\leq 10^{-13}$				
Atmospheric losses, dB	2.8	0.25	0.25	0.55	0.55
Transmitted HAP power per channel in dBm	22.55	25.6	34.6	28.75	37.8
$E_b(\theta_o, \emptyset_o)/N_o$ in dB	14.37	14.34	14.33	14.32	14.32
Channel capacity, in Gbit/s	0.773	0.385	3.086	0.385	3.084

The resulted maximum channel capacity and the required maximum transmitted HAP power to achieve an acceptable bit error probability or rate of 10^{-13} are listed in Table 2 for the three operational frequencies. The channel capacity may reach more than 3 Gbps at the mm-wave frequencies 28 and 39 GHz if a maximum of 400 MHz channel bandwidth is used and the minimum capacity 385 Mbps is obtained if the channel bandwidth is reduced to 50 MHz at these frequencies. For 3.5 GHz frequency, the channel capacity 773 Mbps at 100 MHz bandwidth. These channels are powered with the minimum required transmitted power to achieve the acceptable bit error rate where at 3.5 GHz the channel is powered with 0.18 Watt (22 dBm) while it is about 6 Watt (37.8 dBm) for the 39 GHz carrier with 400 MHz bandwidth.

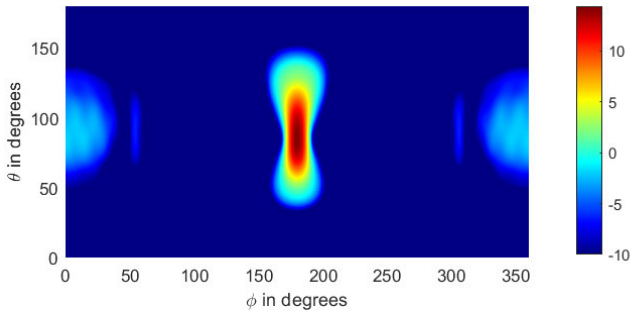

FIGURE 14. Spatial $E_b(\theta, \emptyset)/N_o$ in dB for the bidirectional beamforming system (clipped at −10 dB).

The spatial variations of $E_b(\theta, \emptyset)/N_o$ and the corresponding probability of bit error are shown in Figs. 14 and 15 respectively for a mainlobe generated with the same parameters as in Table 1 for the 3.5 GHz frequency.

The levels of $E_b(\theta, \emptyset)/N_o$ are clipped at -10 dB to clearly investigate the operational levels toward the aircraft. On the other hand, the spatial probability of bit error shown in Fig. 15 has a minimum value of about 6.9×10^{-14} at the

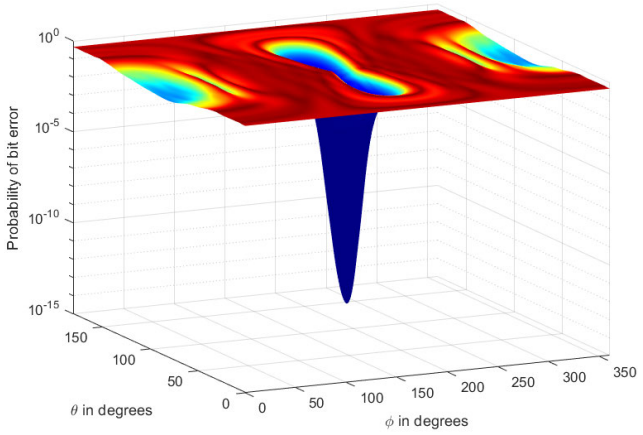

FIGURE 15. Spatial probability of bit error for the bidirectional beamforming system.

mainlobe direction with the aircraft. The required transmitted power per channel to achieve this performance level is only 0.18 Watt or 22.55 dBm and this is due to the dual (bidirectional) gain provided at the aircraft and HAP assuming the same array structure and antenna weighting profile, noting that this transmitted power is required at the end-of-coverage contour while at shorter LOS paths, it may be further reduced.

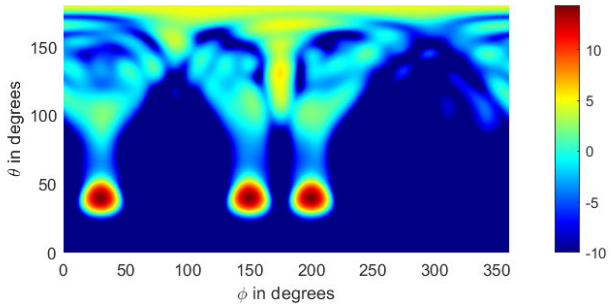

FIGURE 16. Spatial $E_b(\theta, \emptyset)/N_o$ in dB for the bidirectional multibeam connection (clipped at −10 dB).

B. MULTIBEAM AIRCRAFT-HAP COMMUNICATION PERFORMANCE

The analysis in the previous section can be extended for multibeam communication scenario where the aircraft and HAP beamforming system generate multibeams to enhance the communication performance. As shown in Fig. 16 the special variation of $E_b(\theta, \emptyset)/N_o$ for three beams generated at $(40°, 30°)$, $(40°, 150°)$, and $(40°, 200°)$ from HAP toward three in-range aircrafts using the same parameters as in Table 1 at 3.5 GHz except the mainlobe direction. The resulting capacity is the same as for the single generated beam which is 773 Mbps and the corresponding spatial probability of error is shown in Fig. 17 for the three beams which ensure the required level of less than 10^{-13}.

The multibeam generation at an aircraft toward multiple HAPs could be done in the overlap zone where the free space and atmospheric losses are maximum which results in degraded communication link performance. On the other hand, for HAP, multibeam generation boosts the

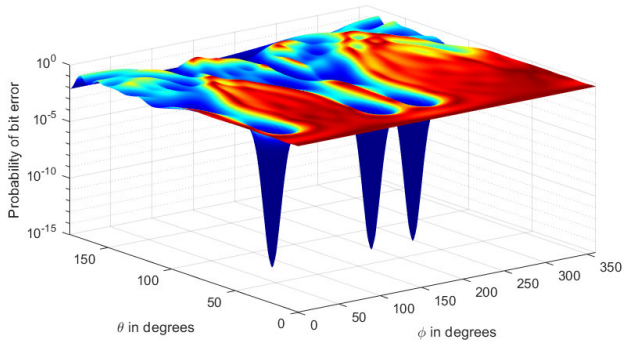

FIGURE 17. Spatial probability of bit error for the bidirectional multibeam connection.

received/transmitted signals with multiple of aircrafts and improves the system capacity and radio resource management. Many in-range aircrafts can share the same radio channel capacity especially if mm-wave frequencies are used.

C. IMPACT OF POINTING ERRORS ON THE SYSTEM PERFORMANCE

The proposed bidirectional beamforming technique boosts the received signals at the aircraft and HAP where each of them provides array gain of 38 dB as shown in the previous section. In this design example, any pointing error in the mainlobe direction either the aircraft or HAP will greatly degrade the system performance if not manipulated properly. For HAPs, station keeping is very important for stable network operation, so, beamforming provides a great advantage to maneuver for this problem. Any positional shift in HAP nominal position should be updated in the GPS service table and all in-range aircrafts should be notified through a broadcast control channel. Also, sudden rotational motion at the aircraft should be manipulated by the onboard antenna beamforming system.

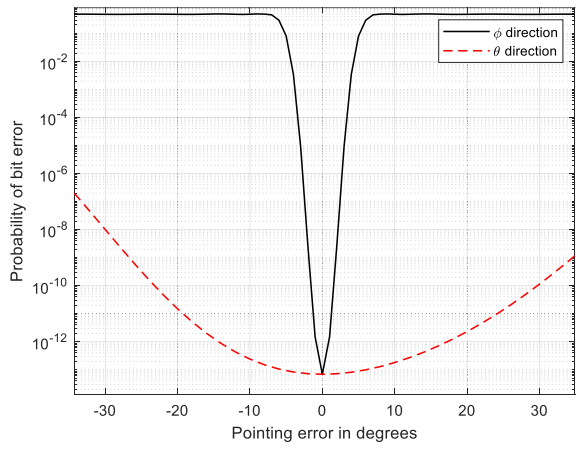

FIGURE 18. Spatial probability of bit error with the beam pointing error in the two directions.

The impact of pointing errors in both directions can be demonstrated through the spatial probability of bit error and $E_b(\theta, \emptyset)/N_o$ as shown in Fig. 17 for 3.5 GHz operational values as listed in Tables 1 and 2. As the beamwidth in the azimuth direction is much narrower than that in the elevation

one, then the system performance will be more sensitive for pointing errors in the azimuth direction as previously demonstrated in Fig 14. The impact of pointing errors on the probability of bit error is clearly demonstrated in Fig. 18, where an error of $\pm 1^\circ$ in the Ø-direction at an aircraft or HAP results in an increase in the probability of error from 6.9×10^{-14} to 1.5×10^{-12}, i.e., an increase of 22 times, while a $\pm 2^\circ$ error results in an increase to 2.66×10^{-9}. The system performance is totally degraded at an error of $\pm 3^\circ$ at which the probability of error is increased to 9.14×10^{-6}. On the other hand, the errors in the θ-direction is not as much impacting as in the Ø-direction where an error of as much high as $\pm 17^\circ$ increases the probability of error to 10^{-12}. Therefore, a fast and adaptive electronic beam steering should be provided by the proposed array to tolerate any positional instabilities by adjusting the mainlobe directions to maintain the best communication performance between an aircraft and HAP. If the antenna at an aircraft is assumed to be omnidirectional, then unidirectional beamforming is done only at HAP which means that there must be a 38 dB compensation in the transmitted power from HAP that requires much larger array size to provide higher transmitting gain and very high transmitted power per channel.

D. IMPACT OF PRACTICAL UNIDIRECTIONAL ANTENNA ELEMENTS ON THE POWER PATTERN

The analysis discussed in the previous sections assumes isotropic antenna elements to demonstrate the impact of the proposed DCCA design and beamforming technique on the radiation pattern, specifically the sidelobe and backlobe radiation levels. On the other hand, if practical antenna models with unidirectional pattern is applied with the proposed DCCA, then the lateral and backward unwanted radiation is expected to be further reduced. Therefore, in this section, a crossed dipole antenna element with perfect conductor backplane is adopted to provide unidirectional radiation pattern with almost isotropic response in one hemisphere to achieve wide angle scanning from the designed DCCA in addition to the reduction in backlobe levels. This antenna element design is shown in Fig. 19 where it is formed by two crossed half wavelength dipoles with one-quarter wavelength separation from a perfect metallic ground plane. The complete specifications of the CCA and DCCA arrays using this unidirectional element are listed in Table 3.

The MATLAB Phased Antenna Array Toolbox has been utilized in the design and simulation process for determining the performance of both the CCA and the proposed DCCA arrays. First, the crossed dipole antenna element is designed using the geometrical dimensions listed in Table 3, then assuming the antenna elements are fixed over a perfect conductor ground plane that extends continuously under the antenna array. The single crossed dipole antenna element performance is shown in Fig. 20 where the power pattern has a large reduction in the backlobe radiation that is relatively at 27 dB approximately below the mainlobe level. This reduced backlobe radiation will be added to the reduction in backlobe

TABLE 3. Crossed dipole concentric circular array and DCCA simulation parameters.

Antenna parameter	Value
Operating frequency	3.5 GHz
Wavelength, λ in mm	85.65 mm
Dipole length	$\lambda/2.1$
Antenna separation from ground plane	$\lambda/4$
Dielectric between antenna and ground plane	air
Ground backplane	Perfect electric conductor
Dipoles offset distance	$\lambda/50$
Dipole width	$\lambda/50$
Feeding location	Center point
Total number of elements	347
Number of circular arrays in concentric circular array	10
Outermost circular array size	63 elements
Number of circular arrays in the outer conical array in the DCCA	4
Number of circular arrays in the inner conical array in the DCCA	7
Outermost circular array size in DCCA	60 elements
Outer conical array base angle	15°
Inner conical array base angle	30°
Mainlobe direction	(45°, 90°)

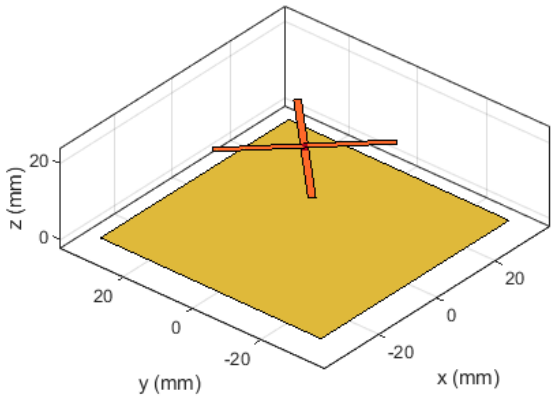

FIGURE 19. Crossed dipole antenna structure with perfect electric conductor ground plane at 3.5 GHz.

radiation resulted from the convexity of the DCCA surface along with the effect of tapered feeding profile in (26).

To investigate the contribution of the proposed DCCA design on the backward and lateral unwanted radiation, a CCA is designed with the same number of elements as the DCCA using crossed dipole unidirectional antenna as displayed in Table 3 and is shown in Fig. 21 (a).

The normalized power pattern from each antenna array structure is examined for the two feeding cases which are the uniform and the sine tapered feeding as proposed in (26) and the results are shown in Figs. 22 and 23.

Fig. 22 (a) displays the normalized power pattern of the crossed dipole CCA array using uniform feeding where the backward radiation is reduced due to the crossed dipole unidirectional pattern. The backward radiation is further minimized when the sine feeding profile in (26) is applied to the antenna elements except an image peak of -33 dB appeared with the same azimuth angle ϕ but at $\theta = 135^\circ$ due to the symmetrical antenna elements distribution. The tapered

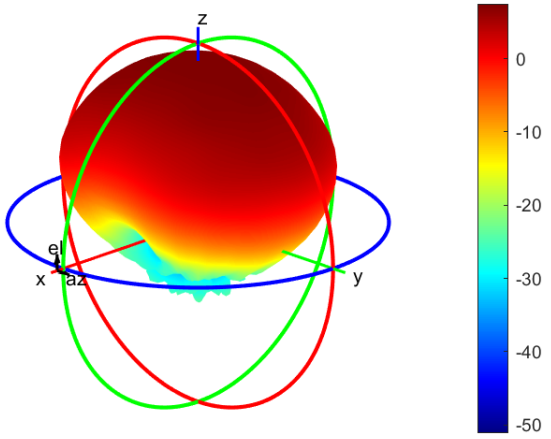

FIGURE 20. Power pattern of crossed dipole antenna with large perfect electric conductor backplane with the design shown in Fig. 19.

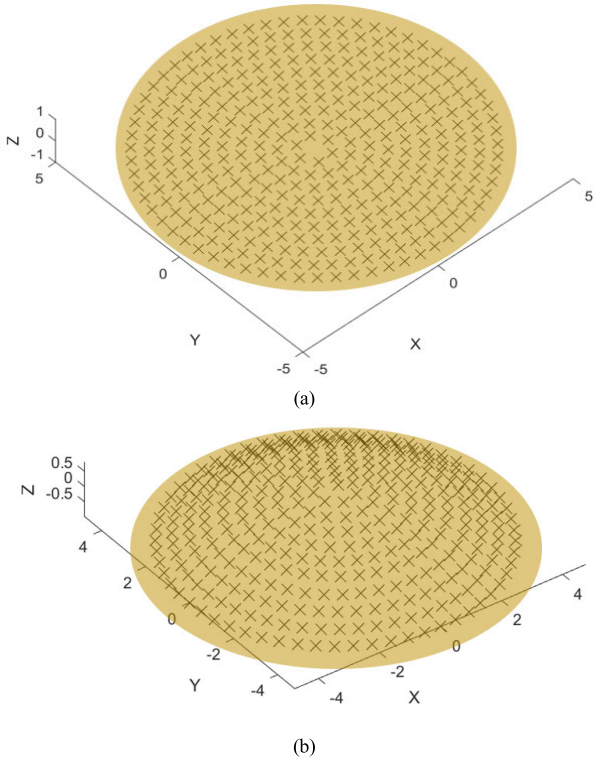

FIGURE 21. Crossed dipole antenna arrays with ground backplane made of perfect conductor: (a) CCA, (b) DCCA. Dimensions are normalized to the wavelength.

feeding has resulted in reducing the sidelobe level to approximately −33 dB.

On the other hand, as shown in Fig. 23 (a) the DCCA array provides a slightly degraded performance in the case of uniform feeding compared with the CCA array due to the reduced effective array area, however as shown in Fig. 23 (b), the convex surface of the DCCA array results in improving the image and backward radiation levels compared to the CCA when applying the proposed tapered sine feeding profile.

The secondary image of the mainlobe appeared in Fig. 23(b) at (135°, 90°) has been reduced to very deep level of −57.6 dB with radiation ring of −46 dB which is

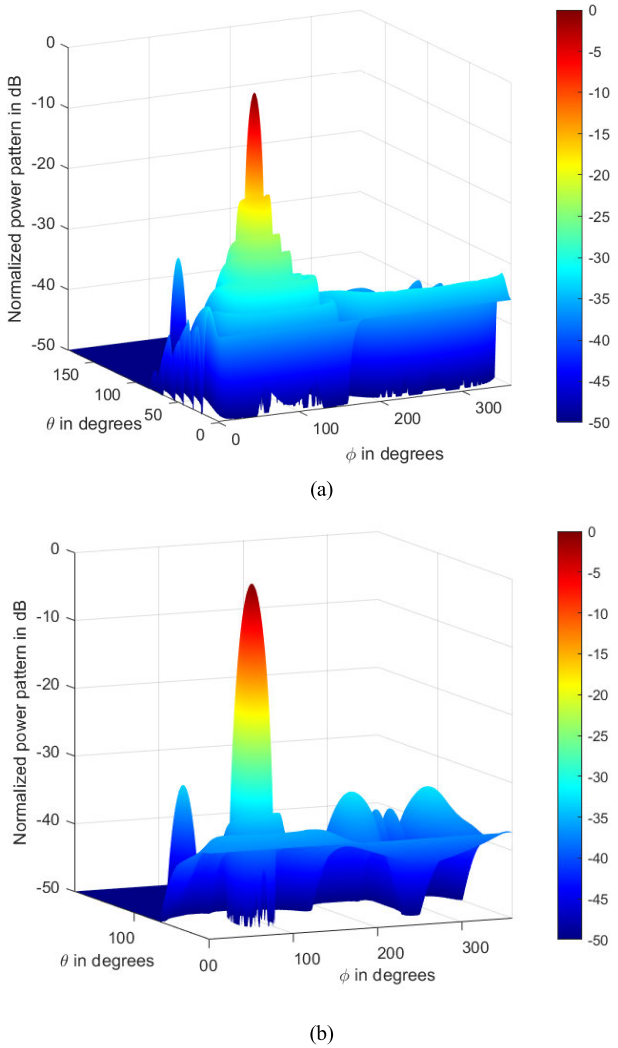

FIGURE 22. Normalized power pattern for crossed dipole CCA with: (a) uniform feeding, (b) tapered sine feeding using (26).

much lower than that appeared when using conventional CCA with the same feeding profile. Therefore, the proposed DCCA provides an add-on reduction in the backward and lateral unwanted radiation levels added to the reduction resulted from the unidirectional antenna elements.

Reducing the unwanted backward and lateral radiation is very necessary for reducing the interference with ground or satellite systems using the same frequency bands. For HAP, the secondary image that appears toward sky results in interference to satellite systems, while backward radiation at 180° azimuth angular separation from the mainlobe direction results in interference with terrestrial systems. The converse for aircraft as the array is heading upward.

The performance comparison results are summarized in Table 4 between CCA and DCCA using unidirectional crossed dipole antenna elements. The main performance improvements obtained from the proposed DCCA compared with the conventional CCA are in the reduction of the sidelobe and backward radiation including the secondary mainlobe image and the backlobe levels which has been confirmed using simulated practical antenna models.

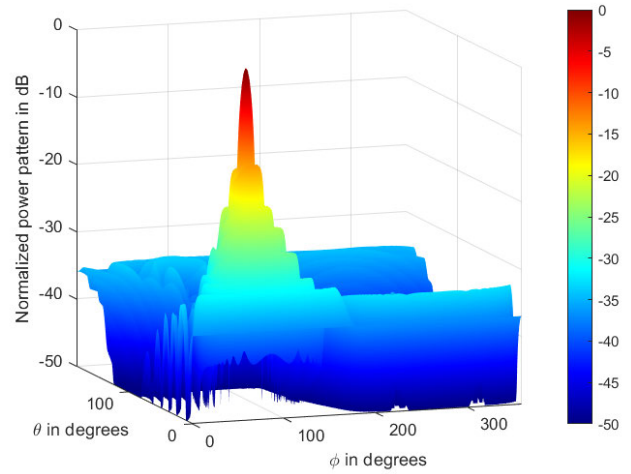

(a)

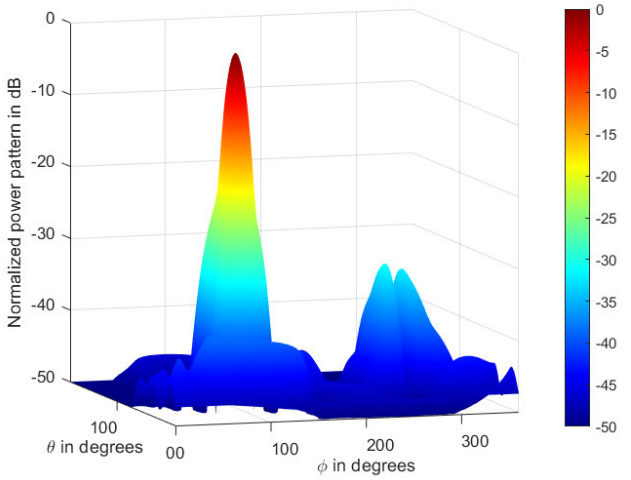

(b)

FIGURE 23. Normalized power pattern for crossed dipole DCCA with: (a) uniform feeding, (b) tapered sine feeding using (26).

TABLE 4. Crossed dipole CCA and DCCA arrays performance comparison.

Radiation levels relative to the mainlobe level	CCA	DCCA
SLL (uniform feeding) in dB	−16.3 dB	−14 dB
Backlobe level (uniform feeding) in dB	−32.2 dB	−35.5 dB
Secondary mainlobe level (uniform feeding) in dB	−33 dB	−57.6 dB
SLL (sine taper feeding)	−33 dB	−38 dB
Backlobe level (sine taper feeding) toward sky in dB	−32.6 dB	−33 dB
Secondary mainlobe level (sine taper feeding) in dB	−33.8 dB	−56.5 dB

VI. CONCLUSION

The aeronautical HAP cellular network for aircrafts has been proposed and discussed in this article using adaptive antenna arrays where the network structure is first demonstrated, then the radio coverage aspects are analyzed, and the communication link performance is improved by developing an adaptive beamforming technique using low-profile dual concentric conical array. The idea of converting the commonly used GPS information of aircrafts and HAP in aviation systems to direction-of-arrival information is investigated where a geometrical model has been proposed based on geocentric coordinate system and a set of conversion equations have been deduced. Then, the radio link between an aircraft and HAP has been improved through the generation of adaptive narrow beams with low sidelobe and backlobe levels at both the aircraft and HAP (bidirectional beamforming) where the antenna elements at each array are fed by adaptive-exponent sine profile.

The exchanged GPS information between aircrafts and HAPs continuously adapt the mainlobe direction generated from onboard beamforming systems to maintain the highest performance of the communication link. When an aircraft enters the overlap region between two HAPs, it may generate multibeam toward the two HAPs to seamlessly handover the communication channels between them and to maintain the highest possible data rate for onboard passengers. Numerical results have shown optimistic performance levels in terms of the required transmission power, bit error rate and channel capacity at the millimeter wave bands of 28 and 39 GHz for the BPSK and QPSK modulation schemes. For stable connection at over the whole HAP coverage zone, the 3.5 GHz can be used with channel capacity of at least 773 Mbps at 100 MHz bandwidth. For above clouds aircraft flights, the higher frequency bands at 28 and 39 GHz could provide channel capacities around 3 Gbps at 400 MHz bandwidth. The probability of bit error rate is kept below 10^{-13} which is acceptable for most applications. In addition, this performance has been investigated for multibeam cases at which the HAP can communicate with several aircrafts to efficiently share the radio resource among in-range aircrafts. Finally, the impact of positional instabilities on the system performance has been demonstrated and discussed where the adaptive beam steering provided by the proposed array at the aircraft and HAP has an important to mitigate these problems and ensure reliable and stable communication performance in the network.

ACKNOWLEDGMENT

This research was supported by Taif University Researchers Supporting Project number (TURSP-2020/161), Taif University, Taif, Saudi Arabia for supporting this work.

REFERENCES

[1] R. D. Apaza and L. Popescu, "The way to the future has already started: ICAO aeronautical telecommunication network (ATN) using Internet protocol suite (IPS) standards and protocol evolution update," in *Proc. IEEE/AIAA 37th Digit. Avionics Syst. Conf. (DASC)*, Sep. 2018, pp. 1170–1175.

[2] D. G. Depoorter, O. Raissouni, E. T. Garriga, and O. Lucke, "The across testbed for the future aeronautical data communications," in *Proc. Integr. Commun. Navigat. Surveill. (ICNS)*, Herndon, VA, USA, 2016, pp. 7D1-1–7D1-13.

[3] A. S. Alam, Y.-F. Hu, P. Pillai, K. Xu, and J. Baddoo, "Optimal datalink selection for future aeronautical telecommunication networks," *IEEE Trans. Aerosp. Electron. Syst.*, vol. 53, no. 5, pp. 2502–2515, Oct. 2017, doi: 10.1109/TAES.2017.2701918.

[4] M. Ehammer and F. Bennison, "Internet protocol for aeronautical communications," in *Proc. IEEE Int. Conf. Ind. Technol. (ICIT)*, Cape Town, South Africa, Feb. 2013, pp. 1315–1320, doi: 10.1109/ICIT.2013.6505863.

[5] Y. Cheng, K. Xu, Y. F. Hu, P. Pillai, J. Baddoo, A. Smith, M. Ali, and A. Pillai, "Technology demonstrator of a novel software defined radio-based aeronautical communications system," *IET Sci., Meas. Technol.*, vol. 8, no. 6, pp. 370–379, Nov. 2014.
[6] M. A. Campos Paiva, R. Amorim Silva, C. Afonso Fleury, and A. Anzaloni, "Design of a novel architecture signaling network to provide Internet multimedia subsystem services through aeronautical passenger communication," *IEEE Latin Amer. Trans.*, vol. 13, no. 7, pp. 2356–2365, Jul. 2015.
[7] I. Gheorghisor, V. Lakshminarayan, L. Globus, D. Arnstein, and F. Box, "Analyses and simulations for aeronautical mobile airport communications system," in *Proc. Integr. Commun. Navigat. Surveill. (ICNS)*, Herndon, VA, USA, 2016, pp. 2C2-1–2C2-13, doi: 10.1109/ICNSURV.2016.7486332.
[8] O. F. P. Ortiz, "Final results of simulations of an aeronautical telecommunications network for ground to ground subnet applications," in *Proc. Integr. Commun. Navigat. Surveill. (ICNS)*, Herndon, VA, USA, 2016, pp. 7C2-1–7C2-11, doi: 10.1109/ICNSURV.2016.7486372.
[9] P. Jacob, R. P. Sirigina, A. S. Madhukumar, and V. A. Prasad, "Cognitive radio for aeronautical communications: A survey," *IEEE Access*, vol. 4, pp. 3417–3443, 2016.
[10] C. Zhang, Y. Zhang, J. Xiao, and J. Yu, "Aeronautical central cognitive broadband air-to-ground communications," *IEEE J. Sel. Areas Commun.*, vol. 33, no. 5, pp. 946–957, May 2015, doi: 10.1109/JSAC.2014.2361089.
[11] J. Zhang, T. Chen, S. Zhong, J. Wang, W. Zhang, X. Zuo, R. G. Maunder, and L. Hanzo, "Aeronautical ad hoc networking for the Internet-above-the-clouds," *Proc. IEEE*, vol. 107, no. 5, pp. 868–911, May 2019.
[12] K.-D. Buchter, "Availability of aeronautical ad-hoc network in different global air transport fleet scenarios," in *Proc. Ind Gen. Assem. Sci. Symp. Int. Union Radio Sci. (URSI GASS)*, Aug. 2017, pp. 1–4.
[13] N. Agrawal and S. J. Darak, "Performance analysis of reconfigurable filtered OFDM for LDACS," in *Proc. 11th Int. Conf. Commun. Syst. Netw. (COMSNETS)*, Jan. 2019, pp. 500–503.
[14] M. A. Bellido-Manganell and M. Schnell, "Towards modern air-to-air communications: The LDACS A2A mode," in *Proc. IEEE/AIAA 38th Digit. Avionics Syst. Conf. (DASC)*, San Diego, CA, USA, Sep. 2019, pp. 1–10, doi: 10.1109/DASC43569.2019.9081678.
[15] A. Bilzhause, B. Belgacem, M. Mostafa, and T. Graupl, "Datalink security in the L-band digital aeronautical communications system (LDACS) for air traffic management," *IEEE Aerosp. Electron. Syst. Mag.*, vol. 32, no. 11, pp. 22–33, Nov. 2017, doi: 10.1109/MAES.2017.160282.
[16] O. Osechas and G. Berz, "Improving the availability of LDACS-based APNT with air-to-air ranging," in *Proc. IEEE/ION Position, Location Navigat. Symp. (PLANS)*, Savannah, GA, USA, Apr. 2016, pp. 91–99, doi: 10.1109/PLANS.2016.7479687.
[17] O. F. Pico Ortiz, "Design, implementation and performance validation of an IP based aeronautical telecommunications network using satellite links," in *Proc. Integr. Commun. Navigat. Surveill. (ICNS)*, Herndon, VA, USA, 2016, pp. 7D2-1–7D2-10, doi: 10.1109/ICNSURV.2016.7486376.
[18] Y. Cheng, K. J. Xu, A. Pillai, P. Pillai, Y. F. Hu, M. Ali, and A. Ahmed, "A realization of integrated satellite-terrestrial communication networks for aeronautical services via joint radio resource management," in *Proc. Pers. Satell. Services (PSATS)*, vol. 123, 2013, pp. 26–37.
[19] *Gogo ATG-4 System*. Accessed: Feb. 12, 2021. [Online]. Available: https://www.engadget.com/2012-11-12-engadget-tours-gogos-flying-test-plane-tries-its-improved-atg.html
[20] *Nokia Broadband ATG Connection*. Accessed: Feb. 12, 2021. [Online]. Available: https://onestore.nokia.com/asset/
[21] *Inmarsat Satellite Network*. Accessed: Feb. 12, 2021. [Online]. Available: https://www.inmarsat.com/
[22] *OneWeb Broadband Internet*. Accessed: Feb. 12, 2021. [Online]. Available: https://www.oneweb.world/
[23] *Starlink Broadband Internet*. Accessed: Feb. 12, 2021. [Online]. Available: https://www.starlink.com/
[24] Y. Albagory, "Modelling, investigation, and feasibility of stratospheric broadband mm-wave 5G and beyond networks for aviation," *Electronics*, vol. 9, no. 11, p. 1872, Nov. 2020.
[25] S. C. Arum, D. Grace, and P. D. Mitchell, "A review of wireless communication using high-altitude platforms for extended coverage and capacity," *Comput. Commun.*, vol. 157, pp. 232–256, May 2020.
[26] F. A. D'Oliveira, F. C. L. D. Melo, and T. C. Devezas, "High-altitude Platforms–Present situation and technology trends," *J. Aerosp. Technol. Manage.*, vol. 8, no. 3, pp. 249–262, Aug. 2016.
[27] M. Guan, Z. Wu, Y. Cui, X. Cao, L. Wang, J. Ye, and B. Peng, "Efficiency evaluations based on artificial intelligence for 5G massive MIMO communication systems on high-altitude platform stations," *IEEE Trans. Ind. Informat.*, vol. 16, no. 10, pp. 6632–6640, Oct. 2020.
[28] M. Guan, Z. Wu, Y. Cui, X. Cao, L. Wang, J. Ye, and B. Peng, "Multi-beam coverage and beamforming technology for high altitude platform station communication system," *EURASIP J. Wireless Commun. Netw.*, vol. 2019, no. 1, pp. 1–10, Dec. 2019.
[29] B. P. Kumar and G. R. Branner, "Design of unequally spaced arrays for performance improvement," *IEEE Trans. Antennas Propag.*, vol. 47, no. 3, pp. 511–523, Mar. 1999, doi: 10.1109/8.768787.
[30] Y. Albagory and O. Said, "Optimizing concentric circular antenna arrays for high-altitude platforms wireless sensor networks," *Int. J. Comput. Netw. Inf. Secur.*, vol. 6, no. 5, pp. 1–8, Apr. 2014.
[31] M. I. Dessouky, H. A. Sharshar, and Y. A. Albagory, "Efficient sidelobe reduction technique for small-sized concentric circular arrays," *Prog. Electromagn. Res.*, vol. 65, pp. 187–200, 2006.
[32] M. Dessouky, H. Sharshar, and Y. Albagory, "A novel tapered beamforming window for uniform concentric circular arrays," *J. Electromagn. Waves Appl.*, vol. 20, no. 14, pp. 2077–2089, Jan. 2006.
[33] E. I. Elsaidy, M. I. Dessouky, S. Khamis, and Y. A. Albagory, "Concentric circular antenna array synthesis using comprehensive learning particle swarm optimizer," *Prog. Electromagn. Res. Lett.*, vol. 29, pp. 1–13, 2012.
[34] Y. A. Albagory, M. Dessouky, and H. Sharshar, "An approach for low sidelobe beamforming in uniform concentric circular arrays," *Wireless Pers. Commun.*, vol. 43, no. 4, pp. 1363–1368, Nov. 2007.
[35] M. Nofal, S. Aljahdali, and Y. Albagory, "Simplified sidelobe reduction techniques for concentric ring arrays," *Wireless Pers. Commun.*, vol. 71, no. 4, pp. 2981–2991, Aug. 2013.
[36] M. Dessouky, H. Sharshar, and Y. Albagory, "An approach for dolph-chebyshev uniform concentric circular arrays," *J. Electromagn. Waves Appl.*, vol. 21, no. 6, pp. 781–794, Jan. 2007.
[37] S. Aljahdali, M. Nofal, and Y. Albagory, "A modified array processing technique based on kaiser window for concentric circular arrays," in *Proc. Int. Conf. Multimedia Comput. Syst.*, Tangiers, Morocco, May 2012, pp. 458–461, doi: 10.1109/ICMCS.2012.6320135.
[38] Y. Albagory, "Direction-independent and self-reconfigurable spherical-cap antenna array beamforming technique for massive 3D MIMO systems," *Wireless Netw.*, vol. 26, no. 8, pp. 6111–6123, Jul. 2020.
[39] I. Radnovic, A. Nesic, and B. Milovanovic, "A new type of turnstile antenna," *IEEE Antennas Propag. Mag.*, vol. 52, no. 5, pp. 168–171, Oct. 2010, doi: 10.1109/MAP.2010.5687522.
[40] G. Pan, Y. Li, Z. Zhang, and Z. Feng, "Isotropic radiation from a compact planar antenna using two crossed dipoles," *IEEE Antennas Wireless Propag. Lett.*, vol. 11, pp. 1338–1341, Nov. 2012.
[41] I. Yoon and H. Ling, "Design of an electrically small circularly polarised turnstile antenna and its application to near-field wireless power transfer," *IET Microw., Antennas Propag.*, vol. 8, no. 5, pp. 308–314, Apr. 2014.
[42] S. G. M. Darwish, K. F. A. Hussein, and H. A. Mansour, "Circularly polarized crossed-dipole turnstile antenna for satellites," in *Proc. 21st Nat. Radio Sci. Conf. (NRSC)*, Cairo, Egypt, 2004, p. B17-1.
[43] J. Proakis and M. Salehi, *Digital Communications*. New York, NY, USA: McGraw-Hill, Nov. 2007.
[44] *Radio Communication Sector of International Telecommunication Union. Attenuation by Atmospheric Gases and Related Effects*, document ITU-R P. 676-10, ITU, Geneva, Switzerland, 2019.
[45] *Radio Communication Sector of International Telecommunication Union. Attenuation Due to Clouds and Fog*, Document ITU-R P. 840-8, ITU, Geneva, Switzerland, 2019.

YASSER ALBAGORY received the Ph.D. degree in communications engineering from the Faculty of Electronic Engineering, Menoufia University, Egypt, in 2008, in the field of high-altitude platform wireless communications system. He is currently an Associate Professor with the Department of Electronics and Electrical Communications Engineering, Faculty of Electronic Engineering, Menoufia University. In 2012, he has joined the Department of Computer Engineering, College of Computers and Information Technology, Taif University, Saudi Arabia. He has published many articles in international journals and conferences in the field of adaptive antenna arrays, mobile communications, high-altitude platforms, drone communications, the IoT, image processing, and sensor networks. He is a Reviewer of many international journals and conferences and has published six books in the field of antenna arrays, high-altitude platforms, and the IoT.